Dense core formation in supersonic turbulent converging flows

Hao Gong and Eve Ostriker (University of Maryland, USA)

Abstract

We present results from numerical simulations of dense core formation in converging, turbulent flows within Giant Molecular Clouds (GMCs). We study how filaments and cores develop in stagnant, post-shock layers. Filaments and cores form simultaneously, and have lower internal velocity dispersions than their surroundings. Core collapse is found to be similar to that for spherical cores, approaching the Larson-Penston solution. We also evaluate how core properties depend on the inflow Mach number, $M = v_{in}/c_s$. Gravitational instability theory predicts that the first core to collapse will have mass proportional to $M^{-1/2}$ and the minimum core mass at late times will be proportional to M^{-1}. Our simulations show that the median core mass lies between these two relations. We develop and test a new method for core identification that uses the gravitational potential computed from the projected surface density. For our simulations, we find that masses and areas found using this method agree with cores identified using the 3D gravitational potential. This offers a new way to identify gravitationally-bound cores in observed GMCs.

1. INTRODUCTION

The core mass function (CMF) is strikingly similar to the stellar initial mass function (IMF), so understanding how cores form is key to understanding the IMF. Observations (e.g. Di Francesco et al. 2007, PPV; Ward-Thompson et a. 2007, PPV) of dense core properties -- such as core density and velocity profiles, and accretion rates – provide constraints on core formation models. Gong & Ostriker (2009, ApJ, 699, 230) developed a unified model of dense core formation and collapse for regions of converging supersonic flows, based on numerical simulations in spherical geometry. In that work, four stages of core formation were identified: core building, core collapse, envelope infall, and late accretion. We have now extended our previous work, using fully three dimensional simulations of converging, turbulent flows.

2. Set up and perturbation

The large-scale converging flows have v_{in} in the +z and –z directions, for a box of x-y-z size $L_{jeans} \times L_{jeans} \times 0.375\, L_{jeans}$. We run simulations with Mach number $M = |v_{in}/c_s|$ ranging from 1 to 9. For each M, we run 20 simulations with different realizations of the turbulent perturbation spectrum. The turbulent amplitude increases with M such that $\Delta v \propto L^{1/2}$.

3. Filament and core development

Within the stagnant post-shock layer, regions with higher initial density develop into long, thin filaments, within which cores grow and then collapse. The gravity of filaments leads to inflows on larger scale, eventually creating sharp fronts where the flow meets the filament and shocks. The line-of-sight velocity dispersions within high density filamentary regions are generally low, and are subsonic in the cores. Figure 1 shows early and late snapshots of surface density and the in-plane velocity components for an M = 5 model. Figure 2 shows an example of line-of-sight surface density, mean velocity, and velocity dispersion at a late stage. Figure 3 shows successive snapshots of the 1D density and velocity profiles of the most evolved core for an M =1.1 model. The central density increases dramatically as the core collapses.

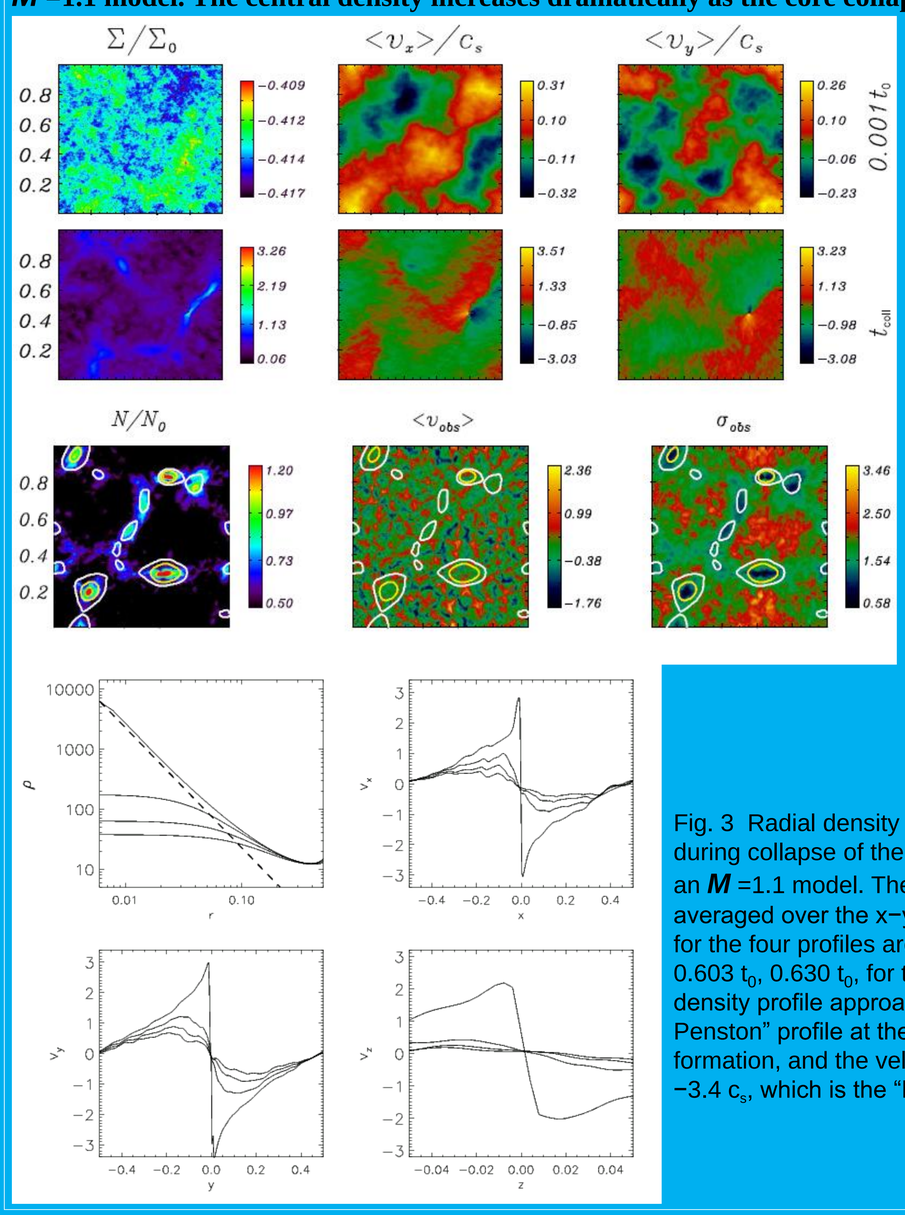

Fig. 1 Surface density and in-plane velocity components projected in the z direction for an M =5 model early in the simulation (upper row), and at the instant of the first core collapse (lower row)

Fig. 2 View of column density, mean velocity, and velocity dispersion in one of the M =5 Models. The contours show cores defined by the gravitational potential. Note that the core regions have low internal velocity Dispersions.

Fig. 3 Radial density and velocity profiles during collapse of the most evolved core for an M =1.1 model. The density profiles are averaged over the x−y plane. The instants for the four profiles are 0.549 t_0, 0.576 t_0, 0.603 t_0, 0.630 t_0, for $t_0 = L_{Jeans}/c_s$. The density profile approaches the "Larson-Penston" profile at the instant of protostar formation, and the velocities v_x, v_y approach −3.4 c_s, which is the "Larson-Penston" limit.

4. A new way of finding cores

Core-finding algorithms affect the properties of the cores that are identified, including mass and radius. When the gravitational potential, rather than the density, is used, there is a natural boundary for each core: the largest closed contour surrounding each minimum in the potential. The gravitational potential can be computed using either the 3D volume density or 2D projected surface density for simulation "data" and the 2D projected surface density for observational data. Figure 4 shows the comparison of core-finding for four different random perturbation realizations of the M = 5 model at the instant of first core collapse. Except for a few small, shallow cores, the core-finding algorithms in 2D and 3D give quite similar results.

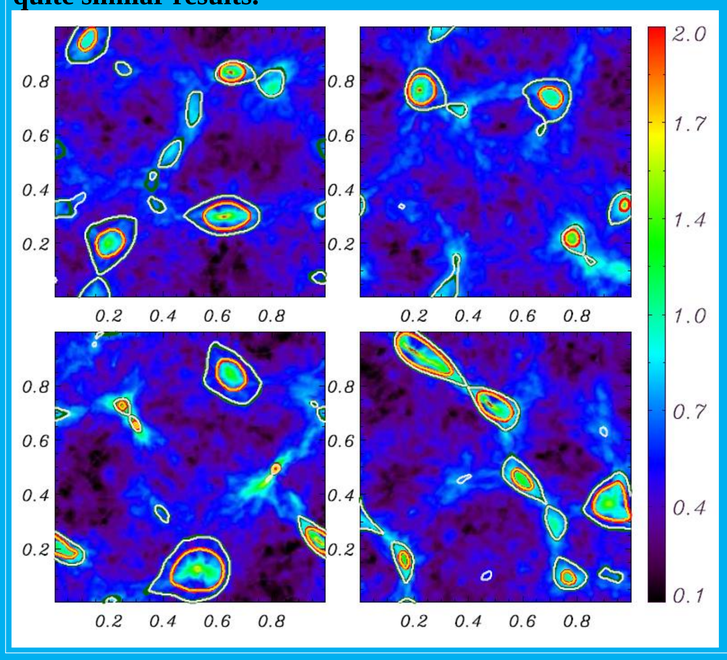

Fig. 4 Comparison of 3D and 2D core-finding for four different M =5 models. The green (or white) curves are core boundaries defined by the largest closed contour of the 3D (or 2D) gravitational potential surrounding each potential minimum. The inner red (or yellow) curves mark the bound core regions, where $E_{th} + E_g < 0$, for each core. Here, E_g is the depth of the potential relative to the largest closed contour of the gravitational potential. The bound regions identified by our 2D and 3D core-finding algorithms agree quite well.

5 Core mass comparison & histogram comparison

For converging flows with higher Mach number, the shock is stronger and therefore the density of post-shock gas in the stagnant regions is higher. At higher density, the local Jean length and mass is lower. As a consequence, a larger number of small, low-mass cores form in models with higher Mach number. For high-M models, large cores still form. This is evident in Figure 5, comparing individual 2D and 3D core masses, and in Figure 6, comparing histograms of 2D and 3D core masses at each Mach number.

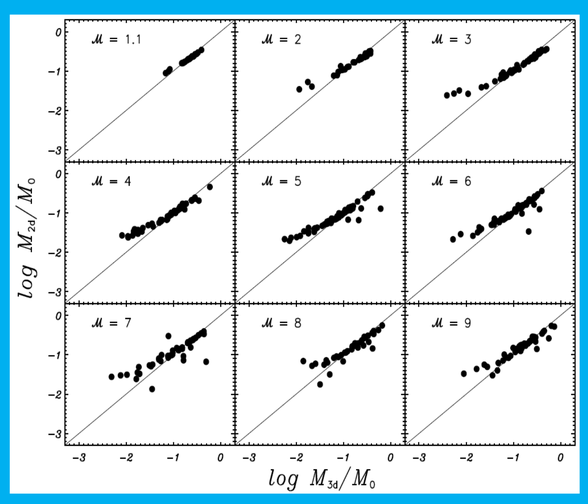

Fig. 5 Core mass from 2D core-finding versus core mass from 3D core-finding. In both cases, only gravitationally bound regions ($E_{th}+E_g < 0$) are included in the core. For bound cores, 2D and 3D masses agree well down to ~ M_{sun}.

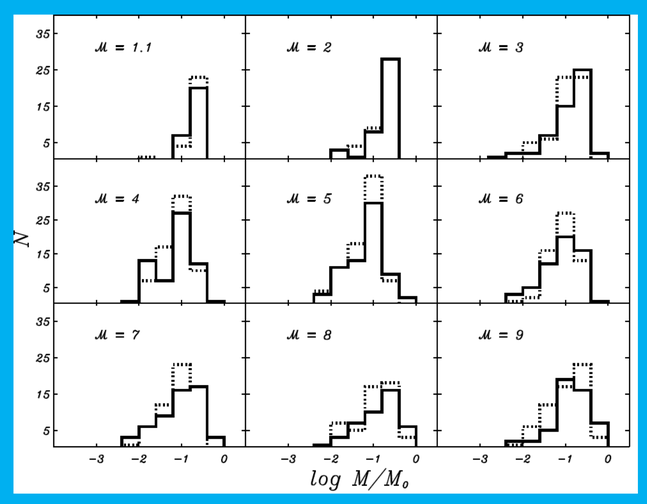

Fig. 6 Histograms of bound core masses found in all simulations for each Mach number. Solid lines are for 3D core-finding and dashed lines are for 2D core-finding. The 2D cores have almost the same distributions as 3D cores. The mass unit is $M_0 = 72\, M_{sun}\, (n_0/100cm^{-3})^{-1/2} (T/10k)^{3/2}$.

6 Core mass and radius as a function of inflow Mach number

Figure 7 shows the median core mass versus Mach number, for cores defined using the largest closed contour of the gravitational potential in either 2D or 3D. We find that the median core mass decreases with increasing inflow Mach number, with a dependence that lies between $M^{-1/2}$ and M^{-1}. Gravitational instability theory predicts the shallower law for the mass of the first core to collapse, and the steeper law for the minimum mass at late stages. Figure 7 shows the median core mass versus M.

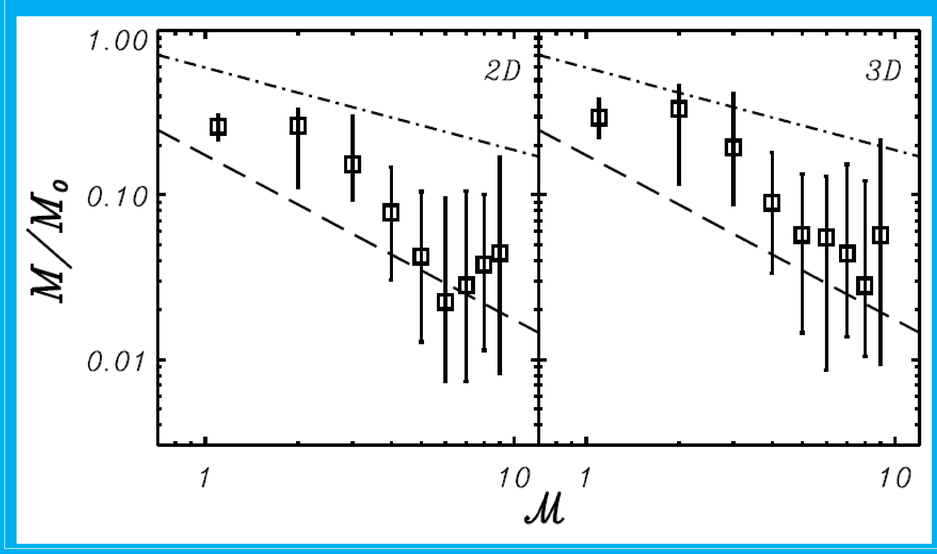

Fig. 7 Median core mass versus Mach number M. The error bars show first and third quartiles of the distribution at each M. The dot-dashed line shows a prediction for the mass of the first core to collapse ($\propto M^{-1/2}$), and the dashed line shows a prediction for the minimum core mass at late times ($\propto M^{-1}$).